Inorg. Chem. **2006**, *45*, 1005–1011

Electronic Effects of Electron-Donating and -Withdrawing Groups in Model Complexes for Iron-Tyrosine-Containing Metalloenzymes

Mauricio Lanznaster,[†] Ademir Neves,*[,†] Adailton J. Bortoluzzi,[†] Aline M. C. Assumpção,[‡] Ivo Vencato,[†] Sergio P. Machado,[‡] and Sueli M. Drechsel[§]

Departamento de Química, Universidade Federal de Santa Catarina, 88040-900 Florianópolis, SC, Brazil, Departamento de Química Inorgânica, Instituto de Química, Universidade Federal do Rio de Janeiro, 21945-970 Rio de Janeiro, RJ, Brazil, and Departamento de Química, Universidade Federal do Paraná, 81531-990 Curitiba, PR, Brazil

Received May 30, 2005

Three new iron(III) complexes with the ligand *N*,*N*′-bis(2-hydroxybenzyl)-*N*,*N*′-bis(pyridin-2-ylmethyl)ethylenediamine, H_2bbpen, containing electron-donating and -withdrawing groups (Me, Br, NO_2) in the 5-position of the phenol rings were synthesized and fully characterized by IR spectroscopy, ESI mass spectrometry, and CHN elemental analyses. X-ray structures of the iron(III) complexes containing NO_2 and Me groups were determined. The effects of the substituents on the electronic properties of the complexes were detected by UV–visible spectroscopy, cyclic voltammetry, and X-ray crystallography. Linear correlations between the Hammett parameter for the substituents (σ_p) and the Fe^{III}/Fe^{II} redox potentials or ligand–metal charge-transfer (LMCT) processes of the complexes were obtained. A theoretical study using DFT is presented and shows good agreement between the experimental and calculated data.

Introduction

The coordination of tyrosine to metal centers is observed in some metalloproteins such as transferrins,[1] lactoferrin,[2] catechol dioxygenases,[3,4] and purple acid phosphatases.[5,6] These iron-tyrosinate proteins show intense colors due to the tyrosinate-to-iron(III) charge-transfer bands,[7] and their enzymatic activity is considered to be related to the Fe^{III}/Fe^{II} potential.[8] A large number of mononuclear high-spin iron(III)-phenolate complexes have been prepared aiming to understand the factors that affect the energy of the tyrosinate-to-iron(III) charge-transfer bands in the proteins and the sensitivity of Fe^{III}/Fe^{II} redox potentials to variations in the ligand donor-atom type.[7,9] Ramesh et al.[10] demonstrated that, in a series of high-spin octahedral iron(III) complexes of Schiff bases, the ligand-to-metal charge-transfer bands shift to higher energies and the Fe^{III}/Fe^{II} redox potentials become more negative as the number of phenolate-containing donor sites increases. Recently, we reported the new ligand H_2bbpen [*N*,*N*′-bis(2-hydroxybenzyl)-*N*,*N*′-bis(pyridin-2-ylmethyl)ethylenediamine] and its manganese(III), vanadium(III), oxo-

* Corresponding author. E-mail: ademir@qmc.ufsc.br.
† Universidade Federal de Santa Catarina.
‡ Universidade Federal do Rio de Janeiro.
§ Universidade Federal do Paraná.

(1) Bailey, S.; Evans, R. W.; Garratt, R. C.; Gorinsky, B.; Hasnain, S.; Horsburgh, C.; Jhoti, H.; Lindley P. F.; Mydin, A.; Sarra, R.; Watson, J. L. *Biochemistry* **1988**, *27* (15), 5804.
(2) Anderson, B. F.; Baker, H. M.; Dodson, E. J.; Norris, G. E.; Rumball, S. V.; Waters, J. M.; Baker, E. N. *Proc. Natl. Acad. Sci. U.S.A.* **1987**, *84*, 1769.
(3) Que, L., Jr.; Lipscomb, J. D.; Zimmermann, R.; Munck, E.; Orme-Johnson, N. R.; Orme-Johnson, W. H. *Biochim. Biophys. Acta* **1976**, *452* (2), 320.
(4) (a) Que, L., Jr.; Heistand, R. H. II; Mayer, R.; Roe, A. L. *Biochemistry* **1980**, *19*, 2588. (b) Que, L., Jr.; Epstein, R. M. *Biochemistry* **1981**, *20* (9), 2545.
(5) Kurts, D. M., Jr. *Chem. Rev.* **1990**, *90* (4), 585−606.
(6) Averill, B. A.; Davis, J. C.; Burman, S.; Zirino, T.; Sanders-Loehr, J.; Loehr, T. M.; Sage, J. T.; Debrunner, P. G. *J. Am. Chem. Soc.* **1987**, *109* (12), 3760.
(7) Ainscough, E. W.; Brodie, A. M.; Plowman, J. E.; Brown, K. L.; Addison, A. W.; Gainsford, A. R. *Inorg. Chem.* **1980**, *19* (12), 3655.
(8) Bradley, F. C.; Lindstedt, S.; Lipscomb, J. D.; Que, L., Jr.; Roe, A. L.; Rundgren, M. *J. Biol. Chem.* **1986**, *261* (25), 11693.
(9) Pyrz, J. W.; Roe, A. L.; Stern, L. J.; Que, L., Jr. *J. Am. Chem. Soc.* **1985**, *107* (3), 614.
(10) Ramesh, K.; Mukherjee, R. *J. Chem. Soc., Dalton Trans.* **1992**, *1*, 83.
(11) (a) Neves, A.; Erthal, S. M. D.; Vencato, I.; Ceccato, A. S.; Mascarenhas, Y. P.; Nascimento, O. R.; Hörner, M.; Batista, A. A. *Inorg. Chem.* **1992**, *31* (23), 4749. (b) Neves, A.; Vencato, I.; Drechsel Erthal, S. M. *Inorg. Chim. Acta* **1997**, *262* (1), 77. (c) Neves, A.; Ceccato, A. S.; Erthal, S. M. D.; Vencato. I. *Inorg. Chim. Acta* **1991**, *187*, 119. (d) Neves, A.; Ceccato, A. S.; Erasmus-Buhr, C.; Gehring, S.; Haase, W.; Paulus, H.; Nascimento, O. R.; Batista, A. A. *J. Chem. Soc., Chem. Commun.* **1993**, *23*, 1782. (e) Neves, A.; Brito, M. A.; Oliva, G.; Nascimento, O. R.; Panepucci, E. H.; Souza, D. H. F.; Batista, A. A. *Polyhedron* **1995**, *14* (10), 1307.

10.1021/ic050869o CCC: $33.50
Published on Web 01/07/2006

Scheme 1. Syntheses of H_2bbpen-X (X = NO_2, Br, H, CH_3)

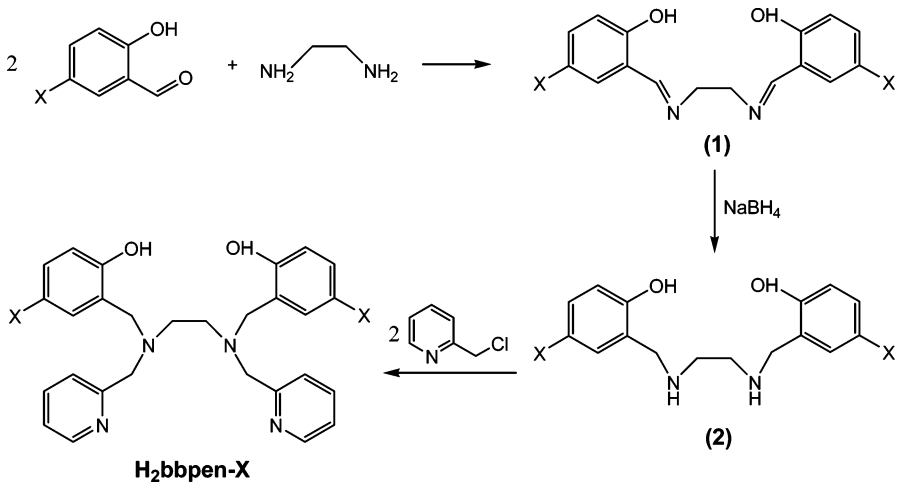

vanadium(IV), and ruthenium(III) complexes.[11] In this article, we present a new series of ligands based on H_2bbpen containing electron-donating and -withdrawing groups and studies on the spectroscopic, electrochemical, and theoretical properties of its iron(III) complexes.

Experimental Section

Abbreviations. The following abbreviations are used in this work: H_2bbpen, *N*,*N*′-bis-(2-hydroxybenzyl)-*N*,*N*′-bis-(pyridin-2-ylmethyl)ethylenediamine; H_2bbpen-Br, *N*,*N*′-bis-(2-hydroxy-5-bromo-benzyl)-*N*,*N*′-bis-(pyridin-2-ylmethyl)ethylenediamine; H_2bbpen-NO_2, *N*,*N*′-bis-(2-hydroxy-5-nitro-benzyl)-*N*,*N*′-bis-(pyridin-2-ylmethyl)ethylenediamine; H_2bbpen-Me, *N*,*N*′-bis-(2-hydroxy-5-methyl-benzyl)-*N*,*N*′-bis-(pyridin-2-ylmethyl)ethylenediamine; H_2BBPPNOL, *N*,*N*′-bis(2-hydroxybenzyl)-*N*,*N*′-bis-(pyridylmethyl)]-2-hydroxy-1,3-propanediamine; H_3BBPMP, 2,6-bis[(2-hydroxybenzyl)(2-pyridylmethyl)aminomethyl]-4-methylphenol; HBPMP, 2,6-bis-[(bis-(2-pyridylmethyl)amino)-methyl]-4-methylphenol; $TBAPF_6$, tetra-*n*-butylammonium hexafluorophosphate; CV, cyclic voltammetry; LMCT, ligand-to-metal charge transfer; MLCT, metal-to-ligand charge transfer.

Materials. $TBAPF_6$, $Fe(ClO_4)_3 \cdot xH_2O$, 2-aminomethylpyridine, pyridine-2-carboxaldehyde, salicylaldehyde, 5-bromosalicylaldehyde, 5-nitrosalicylaldehyde, 5-methylsalicylaldehyde, sodium borohydride, and 2-(chloromethyl)pyridine hydrochloride were obtained from Sigma-Aldrich or Acros. For the electrochemical and spectroscopic studies, high-purity solvents were used as received from Merck, Carlo Erba, and Mallinckrodt. High-purity argon was used to deoxygenate the solutions. All other chemicals and solvents were of reagent grade, were purchased from commercial sources, and were used without prior purification.

Physical Measurements. UV−visible absorption spectra were recorded on a Perkin-Elmer Lambda-19 spectrometer, using 1.0-cm-optical-length quartz cuvettes and acetonitrile as the solvent. Infrared spectra were obtained on a Perkin-Elmer 16PC spectrometer in the range 4000−400 cm^{-1}, in KBr pellets. ^{1}H NMR spectra were obtained with Bruker Ac-200F and Varian U-500 spectrometers, in $CDCl_3$. Elemental analyses were performed on a Carlo Erba E-1110 apparatus. Cyclic voltammograms were obtained on a Princeton Applied Research PAR-273 potentiostat−galvanostat at room temperature under an argon atmosphere. A standard three-component system was used: a carbon-glass working electrode, a platinum wire auxiliary electrode, and a Ag/AgCl reference electrode for organic media. Ferrocene was used as an internal standard ($E_{1/2}$ = 0.40 V vs NHE).[12] All of the complexes were measured using an acetonitrile solution containing 0.1 mol L^{-1} of $TBAPF_6$ as the solvent at 1×10^{-3} mol L^{-1} concentration.

Crystal Structure Determination. A crystal of each complex was selected for X-ray analysis. The intensity data for complexes [Fe(bbpen-NO_2)]ClO_4 and [Fe(bbpen-Me)]ClO_4 were measured with an Enraf-Nonius CAD4 diffractometer at room temperature with graphite-monochromated Mo Kα radiation. The unit cell parameters were determined on the setting angles of 25 centered reflections. All data were corrected for Lorentz and polarization effects. A ψ-scan absorption correction was also applied to the collected intensities with the PLATON program.[13a,b] The structure was solved by direct methods and refined by full-matrix least-squares methods using the SIR97[13c] and SHELXL97[13d] programs, respectively. All non-hydrogen atoms were refined anisotropically. H atoms attached to C atoms were placed at their idealized positions, with C−H distances and U_{eq} values taken from the default settings of the refinement program. For [Fe(bbpen-NO_2)]ClO_4, the H atoms of the water molecule were not found from the difference Fourier map. The figures of the molecular structures were produced with the ORTEP3 program.[13e]

Synthesis of the Ligands. The ligands H_2bbpen-NO_2, H_2bbpen-Br, and H_2bbpen-Me were prepared by modifying the procedure previously reported for H_2bbpen,[14] according to Scheme 1.

(i) H_2bbpen-NO_2. A solution of 5-nitrosalicylaldehyde (2.5 g, 15 mmol) in tetrahydrofuran (25 mL) was treated with ethylenediamine (1.1 mL, 8.0 mmol) and stirred at room temperature. A yellow precipitate (**1-NO_2**) formed immediately and was filtered off and dried under vacuum. Yield: 95%. IR, cm^{-1} (KBr pellet): 1648 (ν C═N); 1610, 1540, 1480, 1446 (ν C═C, C═N, N−O); 1322 (ν N−O); 1216 (ν C−O). To a suspension of **1-NO_2** (2.5 g, 7.0 mmol) in 80 mL of 50% THF/methanol was added sodium borohydride (0.6 g, 16 mmol). The mixture was stirred for 2 h, and HCl (10 mL, 1.0 mol L^{-1}) was added dropwise. A yellow solid

(12) Gagné, R. R.; Koval, C. A.; Lisensky, G. C. *Inorg. Chem.* **1980**, *19*, 2854.

(13) (a) North, A. C. T.; Phillips, D. C.; Mathews, F. S. *Acta Crystallogr.* **1968**, *A24*, 351. (b) Spek, A. L. *Acta Crystallogr.* **1990**, *A46*, C34. (c) Altomare A., Burla M. C., Camalli M., Cascarano G. L., Giacovazzo C., Guagliardi A., Moliterni A. G. G., Polidori G., Spagna R. *J. Appl. Crystallogr.* **1999**, *32*, 115. (d) Sheldrick, G. M. *SHELXL 97, Program for the Refinement of Crystal Structures*; University of Göttingen: Göttingen, Germany, 1997. (e) Farrugia, L. J. *J. Appl. Crystallogr.* **1997**, *30*, 565.

(14) Neves, A.; Ceccato, A. S.; Erthal, S. M. D.; Vencato, I. *Inorg. Chim. Acta* **1991**, *187* (2), 119.

was obtained (**2-NO_2**), filtered off, washed with water and methanol, and dried under vacuum. Yield: 90%. IR, cm^{-1} (KBr pellet): 1597, 1569, 1480 (ν C═C, C═N, N—O); 1333 (ν N—O); 1295 (ν C—O). A suspension of **2-NO_2** (3.0 g, 8.3 mmol) was treated with sodium hydroxide (18 mL, 1.0 mol L^{-1}) and stirred, producing an orange solution. To this solution 2-(chloromethyl)-pyridine hydrochloride (3.3 g, 20 mmol) previously neutralized with NaOH (19.5 mL, 1.0 mol L^{-1}) was added. The reaction mixture was heated at 75 °C for 5 h, and stirred at room temperature for a further 15 h. A yellowish precipitate of H_2bbpen-NO_2 was obtained, filtered off, washed with cold methanol and dried under vacuum. Yield: 80%. IR, cm^{-1} (KBr pellet): 1584, 1510, 1491, 1446 (ν C═C, C═N, N—O); 1332 (ν N—O); 1287 (ν C—O). ^{1}H NMR, ppm (200 MHz, $CDCl_3$): 8.56 (d, 2H), 8.05 (dd, 2H), 7.83 (d, 2H), 7.69 (t, 2H), 7.28−7.22 (m, 2H), 7.08 (d, 2H), 6.79 (d, 2H), 3.77 (s, 4H), 3.72 (s, 4H), 2.71 (s, 4H). Anal. Calcd for $C_{28}H_{28}N_6O_6$: C, 61.76; H, 5.18; N, 15.43%. Found: C, 61.52; H, 5.10; N, 15.51%.

(ii) H_2bbpen-Br. The reaction between 5-bromosalicylaldehyde (10 g, 50 mmol) and ethylenediamine (1.7 mL, 25 mmol) to produce **1-Br** was performed by the same procedure as described above for **1-NO_2**. Yield: 97%. IR, cm^{-1} (KBr pellet): 1653, 1634 (ν C═N); 1568, 1474 (ν C═C, C═N); 1275 (ν C—O). Reduction of **1-Br** (10 g, 23.5 mmol) with sodium borohydride (1.0 g, 26.5 mmol) was performed as described for **2-NO_2**. Yield: 70%. IR, cm^{-1} (KBr pellet): 1584, 1461, 1414 (ν C═C, C═N); 1273 (ν C—O). To a 50% water/THF solution of 2-(chloromethyl)pyridine hydrochloride (4.6 g, 28 mmol) were added sodium bicarbonate (5 g, 50 mmol) and **2-Br** (4.1 g, 9.5 mmol). The reaction mixture was heated at 80 °C for 12 h and then cooled to room temperature. The THF was removed under reduced pressure, and the water was decanted off. The remaining red oil was dissolved in 50% 2-propanol/ethyl acetate and kept at −20 °C for 48 h, forming a white precipitate of H_2bbpen-Br that was filtered off and dried under vacuum. Yield: 65%. IR, cm^{-1} (KBr pellet): 1593, 1469, 1481, 1431 (ν C═C, C═N); 1272 (ν C—O). ^{1}H NMR, ppm (200 MHz, $CDCl_3$): 8.56 (d, 2H), 7.54 (t, 2H), 7.26−7.17 (m, 4H), 7.09 (d, 2H), 6.98 (d, 2H), 6.69 (d, 2H), 3.72 (s, 4H), 3.63 (s, 4H), 2.68 (s, 4H). Anal. Calcd for $C_{28}H_{28}N_4O_2Br_2$: C, 55.08; H, 4.63; N, 9.18%. Found: C, 54.86; H, 4.73; N, 8.99%.

(iii) H_2bbpen-Me. The imine **1-Me** was prepared by the procedure described above for **1-NO_2** using 5-methylsalicylaldehyde (2.0 g, 13 mmol) to react with ethylenediamine (0.44 mL, 6.5 mmol) in methanol. Yield: 99%. IR, cm^{-1} (KBr pellet): 1638 (ν C═N); 1585, 1492 (ν C═C, C═N); 1283 (ν C—O). Reduction of **1-Me** (2.1 g, 6.4 mmol) with sodium borohydride (0.6 g, 16 mmol) was performed as described for **2-NO_2**. Yield: 97%. IR, cm^{-1} (KBr pellet): 1610, 1503, 1471, 1453 (ν C═C, C═N); 1272 (ν C—O). A mixture of **2-Me** (1.5 g, 5 mmol), 2-(chloromethyl)pyridine hydrochloride (2.0 g, 12 mmol), and sodium carbonate (1.3 g, 12 mmol) in 1:1 methanol/water (60 mL) was refluxed for 24 h. After the solvent had been removed, the crude product was recrystallized in a 1:1 mixture of 2-propanol and ethyl acetate. A white powder of H_2bbpen-Me was obtained in 60% yield. IR, cm^{-1} (KBr pellet): 1590, 1500, 1430 (ν C═C, C═N); 1272 (ν C—O). ^{1}H NMR, ppm (500 MHz, $CDCl_3$): 8.56 (d, 2H), 7.61 (dt, 2H), 7.15−7.18 (m, 4H), 6.96 (dd. 2H), 6.73 (d, 2H), 6.70 (s, 2H), 3.75 (s, 4H), 3.65 (s, 4H), 2.75 (s, 4H), 2.225 (s, 6H). Anal. Calcd for $C_{30}H_{34}N_4O_2$: C, 74.66; H, 7.10; N, 11.61; O, 6.63%. Found: C, 74.23; H, 7.18; N, 11.56%.

Synthesis of the Complexes. The iron complexes were prepared by reactions between $Fe(ClO_4)_3 \cdot xH_2O$ and the respective ligands H_2bbpen-NO_2, H_2bbpen-Br, and H_2bbpen-Me by modifying the procedure previously reported for the complexes [Fe(bbpen)]PF_6 and [Fe(bbpen)]NO_3.[15]

(i) [Fe(bbpen-NO_2)]$ClO_4 \cdot H_2O$. To a suspension of H_2bbpen-NO_2 (0.54 g, 1 mmol) in methanol (30 mL) was added $Fe(ClO_4)_3 \cdot xH_2O$ (0.52 g, 1 mmol). The reaction mixture was heated at 50 °C under stirring for 15 min and then cooled to room temperature. The microcrystalline precipitate formed was filtered off, washed with methanol, and dried under vacuum. Recrystallization in acetonitrile/2-propanol yielded X-ray-suitable single crystals of [Fe(bbpen-NO_2)]$ClO_4 \cdot H_2O$. IR, cm^{-1} (KBr pellet): 1604, 1568, 1512, 1474, 1432 (ν C═C, C═N); 1284 (ν C—O). Anal. Calcd for $C_{28}H_{28}N_6O_{11}FeCl$: C, 46.98; H, 3.94; N, 11.74%. Found: C, 47.17; H, 3.80; N, 11.67%. ESI (m/z^+): 582.00, 100% for $[C_{28}H_{26}N_6O_6Fe]^+$.

(ii) [Fe(bbpen-Br)]ClO_4. The complex [Fe(bbpen-Br)]ClO_4 was synthesized following the procedure described above for [Fe(bbpen-NO_2)]$ClO_4 \cdot H_2O$. IR, cm^{-1} (KBr pellet): 1604, 1470, 1412 (ν C═C, C═N); 1276 (ν C—O); 1088 (ν ClO_4^-). Anal. Calcd for $C_{28}H_{26}N_4O_6FeClBr_2$: C, 43.92; H, 3.42; N, 7.32%. Found: C, 43.45; H, 3.24; N, 6.95%. ESI (m/z^+): 665.97, 100% for $[C_{28}H_{26}N_4O_2Br_2Fe]^+$.

(iii) [Fe(bbpen-Me)]ClO_4. The complex [Fe(bbpen-Me)]ClO_4 was synthesized following the procedure described above for [Fe(bbpen-NO_2)]$ClO_4 \cdot H_2O$. IR, cm^{-1} (KBr pellet): 1607, 1569, 1485, 1465, 1444 (ν C═C, C═N); 1264 (ν C—O); 1089 (ν ClO_4^-). Anal. Calcd for $C_{30}H_{32}ClFeN_4O_6$: C, 56.66; H, 5.07; N, 8.81. Found: C, 56.61; H, 5.00; N, 8.89. ESI (m/z^+): 536.11, 100% for $[C_{30}H_{32}FeN_4O_2]^+$.

(iv) [Fe(bbpen)]ClO_4. The complex [Fe(bbpen)]ClO_4 was synthesized following the procedure described above for [Fe(bbpen-NO_2)]$ClO_4 \cdot H_2O$. IR, cm^{-1} (KBr pellet): 1604, 1570, 1477, 1451 (ν C═C, C═N); 1268 (ν C—O); 1088 (ν ClO_4^-). Anal. Calcd for $FeC_{28}H_{30}N_4O_7Cl$: C, 53.73; H, 4.83; N, 8.95. Found: C, 53.81; H, 4.75; N, 8.70. ESI (m/z^+): 508.23, 100% for $[C_{28}H_{28}N_4O_2Fe]^+$.

Results and Discussion

Synthesis. The ligands were synthesized by modifying the procedure previously reported for H_2bbpen.[14] All of them were obtained with good yields and were fully characterized by IR and ^{1}H NMR spectroscopies and elemental analysis. A general procedure was used to synthesize the series of iron(III) complexes through the reaction of the ligands H_2bbpen-NO_2, H_2bbpen-Br, H_2bbpen, and H_2bbpen-Me with $Fe(ClO_4)_3 \cdot xH_2O$. The complexes [Fe(bbpen-NO_2)]$ClO_4 \cdot H_2O$, [Fe(bbpen-Br)]ClO_4, [Fe(bbpen)]ClO_4, and [Fe(bbpen-Me)]ClO_4 were obtained in good yields, and all of them were fully characterized by IR spectroscopy, ESI mass spectrometry, and elemental analysis. Single-crystal X-ray structures were obtained for [Fe(bbpen-NO_2)]ClO_4 and [Fe(bbpen-Me)]ClO_4. Although the cation $[Fe(bbpen)]^+$ has been already reported with NO_3^- and PF_6^- counterions,[15] it was synthesized again as a ClO_4^- salt for a better comparison with the other compounds in the series.

X-ray Structural Characterization. The crystal structures of the complexes [Fe(bbpen-Me)]ClO_4 and [Fe(bbpen-NO_2)]$ClO_4 \cdot H_2O$ were solved. The ORTEP representations are given in Figure 1, and selected bond lengths and angles are listed in Table 1.

The structure of [Fe(bbpen-Me)]ClO_4 consists of a mononuclear cation and an uncoordinated perchlorate anion in a

(15) Setyawati, I. A.; Rettig, S. J.; Orvig, C. *Can. J. Chem.* **1999**, *77*, *7* (12), 2033.

Table 1. Selected Experimental and Calculated Bond Lengths (Å) and Angles (deg) for [Fe(bbpen-NO_2)]ClO_4·H_2O (1), [Fe(bbpen-Br)]ClO_4 (**2**), [Fe(bbpen)]NO_3·MeOH (**3**),[14] and [Fe(bbpen-Me)]ClO_4 (**4**)

	experimental			calculated			
	1	**2**	**4**	**1**	**2**	**3**	**4**
Fe−O1	1.888(3)	1.861(1)	1.873(3)	1.857	1.864	1.859	1.857
Fe−O2	1.889(3)	1.885(1)	1.875(3)	1.858	1.865	1.859	1.857
Fe−N1	2.222(3)	2.234(2)	2.217(4)	2.337	2.319	2.330	2.333
Fe−N2	2.214(3)	2.228(2)	2.253(4)	2.337	2.319	2.330	2.333
Fe−N31	2.146(4)	2.135(3)	2.150(4)	2.210	2.198	2.207	2.207
Fe−N41	2.148(4)	2.135(3)	2.165(4)	2.207	2.196	2.206	2.206
O1−Fe−O2	103.27(12)	103.64(6)	103.59(13)	107.52	106.58	107.12	107.65
O1−Fe−N2	167.09(13)	165.52(7)	164.54(13)	162.42	162.98	162.85	162.34
O1−Fe−N1	89.03(13)	88.91(6)	88.89(14)	87.47	87.81	87.75	87.72
O1−Fe−N31	93.21(14)	93.21(7)	92.89(14)	94.10	93.62	93.88	93.58
O1−Fe−N41	97.11(13)	93.80(7)	99.25(15)	96.10	95.91	96.14	96.38
O2−Fe−N2	87.29(12)	88.77(7)	88.67(13)	87.85	88.01	87.75	87.67
O2−Fe−N1	166.08(13)	164.93(7)	165.47(14)	162.87	163.22	162.85	162.33
O2−Fe−N31	97.42(14)	96.88(7)	94.73(15)	96.01	95.90	96.16	96.33
O2−Fe−N41	93.96(14)	93.37(7)	92.85(14)	94.18	93.63	93.87	93.62
N1−Fe−N31	88.24(14)	90.59(7)	92.02(15)	90.98	91.65	91.18	91.22
N1−Fe−N41	77.83(14)	77.28(7)	77.58(15)	75.59	75.98	75.68	75.61
N1−Fe−N2	81.45(12)	80.04(7)	80.40(14)	78.79	79.32	79.05	78.74
N2−Fe−N31	77.88(16)	77.71(7)	76.51(14)	75.40	75.82	75.68	75.61
N2−Fe−N41	89.43(13	92.85(7)	89.36(14)	91.10	91.76	91.18	91.21
N31−Fe−N41	162.47(13)	165.86(7)	163.77(15)	162.71	164.02	163.09	163.10

general position. The coordination sphere of the iron atom is best described as a distorted octahedron. The two halves of the hexadentate ligand bbpen-Me^{2-} are in a facial arrangement (*fac*-N_2O set) where the two phenolate oxygen and the two amine nitrogen atoms (of the ethylenediamine backbone) coordinate in a cis configuration to the equatorial plane. The remaining pyridine nitrogen atoms, mutually trans, complete the coordination sphere of the iron center. Similar coordination arrangements of the ligands bbpen-$NO_2{}^{2-}$ and bbpen^{2-} were observed in [Fe(bbpen-NO_2)]ClO_4·H_2O and [Fe(bbpen)]-NO_3·CH_3OH, respectively. The latter, reported by Orvig and co-workers,[15] has a nitrate counterion instead of perchlorate, which does not affect the coordination mode of the [Fe(bbpen)]$^+$ cation. Similar coordination arrangements of the ligand bbpen^{2-} were observed in the corresponding [V^{III}(bbpen)]PF_6[14] and [Mn^{III}(bbpen)]PF_6[11a] complexes. However, in [Ru^{III}(bbpen)]PF_6,[11e] one of the phenolate oxygen atoms is coordinated trans to one pyridine, whereas the other phenolate is trans to an amine nitrogen atom.

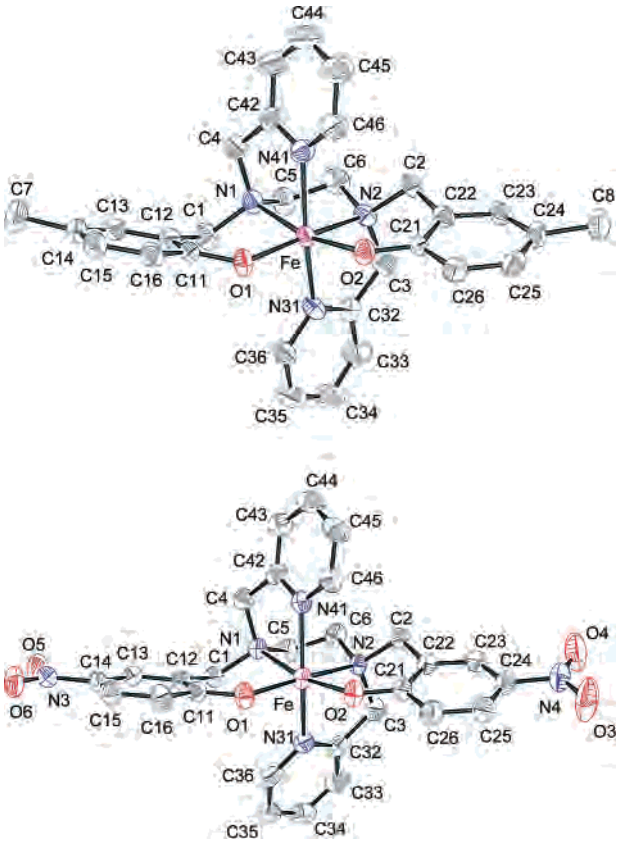

Figure 1. ORTEP diagrams of the cation complexes (top) [Fe(bbpen-Me)]$^+$ and (bottom) [Fe(bbpen-NO_2)]$^+$.

The methyl electron-donating groups in the cation [Fe(bbpen-Me)]$^+$ do not cause considerable changes in bond distances and angles when compared to [Fe(bbpen)]$^+$. However, slightly longer Fe—$O_{phenolate}$ bonds are observed for [Fe(bbpen-NO_2)]$^+$. As a result, the Fe—N_{amine} bond distances decreased a little as a result of the trans effect [16] of the phenolate moieties. The increase in the Fe—$O_{phenolate}$ bond lengths, although small, provides evidence of the electron-withdrawing effect of the nitro groups, which is consistent with the spectroscopic and electrochemical data.

UV−Visible Spectra. The UV−visible spectra of the complexes [Fe(bbpen-NO_2)]ClO_4, [Fe(bbpen-Br)]ClO_4, [Fe(bbpen)]ClO_4, and [Fe(bbpen-Me)]ClO_4 show the presence of three maxima in the region 250−900 nm. The spectral data are summarized in Table 2.

The two lower-energy bands are assigned as being $O_{phenolate}$-to-iron(III) LMCT processes, whereas the highest-energy band is attributed to ligand internal transitions. The spectral data reported by Orvig and co-workers for [Fe(bbpen)]-NO_3[15] are in good agreement with those obtained for [Fe(bbpen)]ClO_4 in this study. According to Orvig and co-workers,[15] the two bands observed for [Fe(bbpen)]NO_3 at 575 nm (ϵ = 5400 mol L^{-1} cm^{-1}) and 323 nm (ϵ = 8900

(16) Shongwe, M. S.; Kaschula, C. H.; Adsetts, M. S.; Ainscough, E. W.; Brodie, A. M.; Morris, M. J. *Inorg. Chem.* **2005**, *44* (9), 3070.

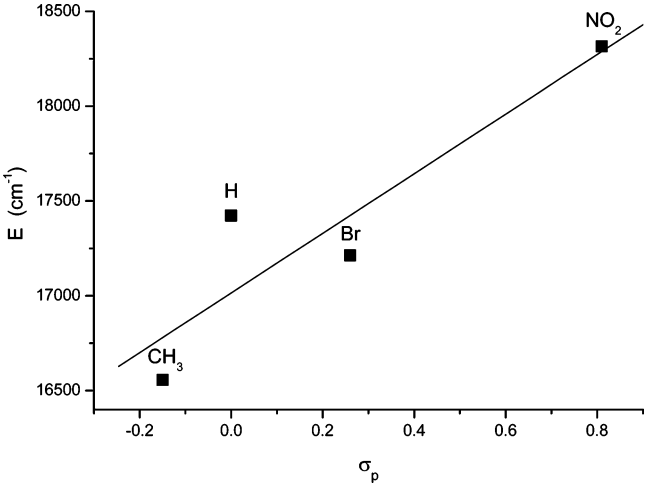

Figure 2. Correlation between the Hammett parameter σ_p[19] for Me, H, Br, and NO_2, and the lowest-energy LMCT process for the complexes [Fe(bbpen-Me)]ClO_4, [Fe(bbpen)]ClO_4, [Fe(bbpen-Br)]ClO_4, and [Fe(bbpen-NO_2)]ClO_4.

Table 2. UV−Visible Spectral Data of the Complexes Measured in MeCN

complex	λ, nm (ϵ, mol^{-1} L^{-1})		
[Fe(bbpen-Me)]ClO_4	284 (11400)	324 (8600)	604 (5700)
[Fe(bbpen)]ClO_4	275 (11500)	322 (7500)	574 (4800)
[Fe(bbpen-Br)]ClO_4	287 (11300)	324 (9000)	581 (5700)
[Fe(bbpen-NO_2)]ClO_4	234 (22800)	350 (29000)	546 (7400)

mol L^{-1} cm^{-1}) are assigned as p$\pi \rightarrow$ dπ* and p$\pi \rightarrow$ dσ* LMCT processes, respectively. This attribution is supported by analogy with other iron(III)-phenolate complexes reported in the literature.[9,10,17,18] A linear correlation between the Hammett parameter σ_p[19] and the energy of the lowest LMCT band of the complexes [Fe(bbpen-NO_2)]ClO_4, [Fe(bbpen-Br)]ClO_4, [Fe(bbpen)]ClO_4, and [Fe(bbpen-Me)]ClO_4 was found. According to the plot in Figure 2, the LMCT process is shifted to a higher energy as the electron-withdrawing effect of the substituent groups increases. Consequently, a hypsochromic shift is observed for [Fe(bbpen-NO_2)]ClO_4, whereas the complex [Fe(bbpen-Me)]ClO_4 shows a bathochromic shift when compared to [Fe(bbpen)]ClO_4. Interestingly, the p$\pi \rightarrow$ dσ* LMCT process that appears in the region of 324 nm does not seem to be affected by the substituents in the bound phenolate groups. The band at 350 nm in the spectrum of [Fe(bbpen-NO_2)]ClO_4 is shifted with respect to the other complexes because of an overlay between the LMCT process and $\pi_{phenolate}$-to-NO_2 intraligand charge transfer, which is also observed in the spectrum of the uncoordinated ligand.

Electrochemistry. The redox behavior of the complexes was studied by cyclic voltammetry (CV). The cyclic voltammograms of [Fe(bbpen-NO_2)]ClO_4, [Fe(bbpen-Br)]ClO_4, [Fe(bbpen)]ClO_4, and [Fe(bbpen-Me)]ClO_4 show one well-defined one-electron reversible wave that is attributed to the Fe^{III}/Fe^{II} redox process. The voltammograms are shown in Figure 3, and the results are summarized in Table 3.

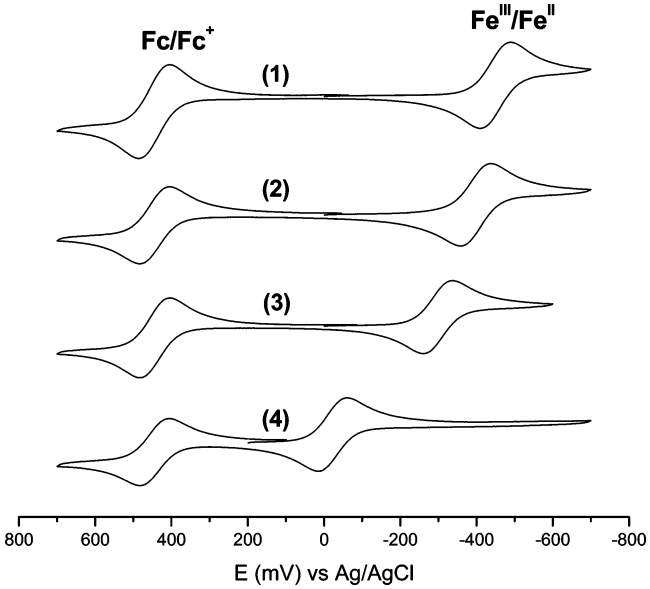

Figure 3. Cyclic voltammograms of (1) [Fe(bbpen-Me)]$^+$, (2) [Fe(bbpen)]$^+$, (3) [Fe(bbpen-Br)]$^+$, and (4) [Fe(bbpen-NO_2)]$^+$ at 100 mV s^{-1}, 1×10^{-3} mol L^{-1} in MeCN with 0.1 mol L^{-1} $TBAPF_6$, using a typical carbon, Ag/AgCl, and Pt wire three-electrode system and ferrocene[12] as the internal standard ($E_{1/2}$ = 444 mV).

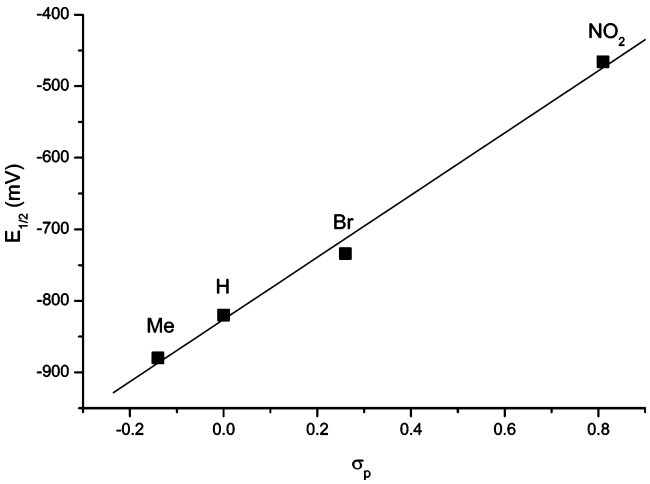

Figure 4. Correlation between the Hammett parameter σ_p[19] and the half-wave potentials ($E_{1/2}$) for [Fe(bbpen-NO_2)]ClO_4, [Fe(bbpen-Br)]ClO_4, [Fe(bbpen)]ClO_4, and [Fe(bbpen-Me)]ClO_4.

Table 3. Cyclic Voltammetry Data for the Iron Complexes at 100 mV s^{-1} in MeCN and the Hammett Parameter σ_p[19] for the Substituent Groups Me, H, Br, and NO_2

complex	σ_p	$E_{1/2}$ (mV)[a]	ΔE_p	i_{pa}/i_{pc}
[Fe(bbpen-Me)]ClO_4	−0.14	−893	80	1.0
[Fe(bbpen)]ClO_4	0.00	−842	78	1.0
[Fe(bbpen-Br)]ClO_4	0.26	−743	76	1.0
[Fe(bbpen-NO_2)]ClO_4	0.81	−482	76	1.0

[a] Potential versus ferrocene[12] ($E_{1/2}$ = 444 mV, ΔE_p = 78 mV, i_{pa}/i_{pc} = 1.0).

As can be observed in Table 3, the half-wave potentials ($E_{1/2}$) of the complexes become more negative in the following sequence of the ligands: bbpen-Me^{2-} > bbpen-H^{2-} > bbpen-Br^{2-} > bbpen-NO_2^{2-}. The influence of the ligands on the redox potential of their corresponding iron

(17) Gaber, B. P.; Miskowski, V.; Spiro, T. G. *J. Am. Chem. Soc.* **1974**, *96* (22), 6868.
(18) Carrano, C. J.; Spartalian, K.; Appa Rao, G. V. N.; Pecoraro, V. L.; Sundaralingan, M. *J. Am. Chem. Soc.* **1985**, *107* (6), 1651.
(19) March, J. *Advanced Organic Chemistry: Reactions, Mechanisms and Structure*, 4th ed.; John Wiley & Sons: New York, 1992.

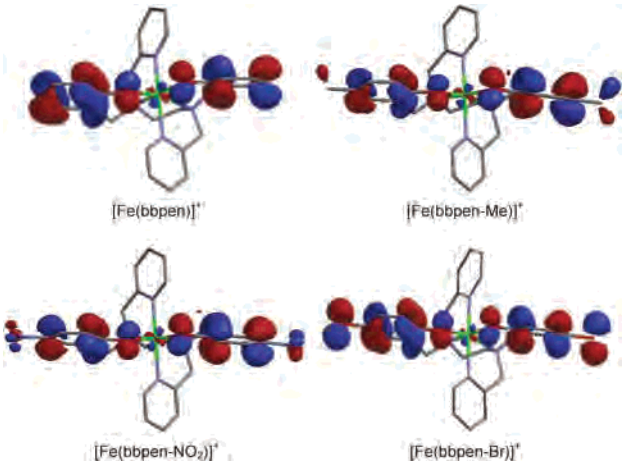

Figure 5. Graphical representations of α-HOMO.

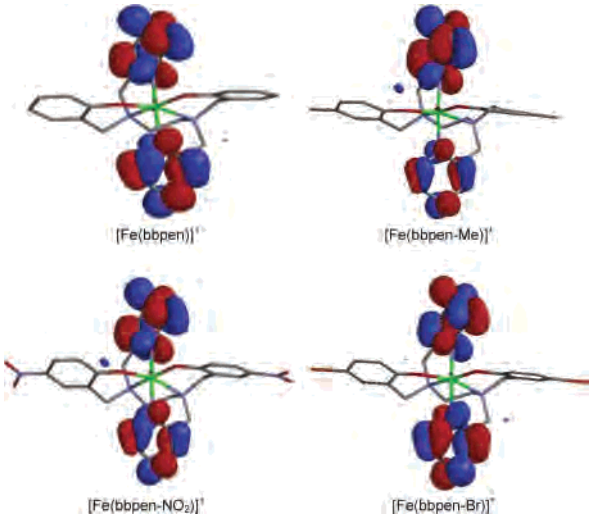

Figure 6. Graphical representations of α-LUMO.

complexes is a clear indication of the effect of the para substituent groups on the donor capacity of the phenolate moieties. Indeed, a linear correlation between the Hammett parameters σ_p[19] and the redox potentials of the Fe^{III}/Fe^{II} couple can be observed in Figure 4. This fact can be interpreted as an increase in the electronic density over the iron center due to the donor effect of the methyl group, resulting in a greater stabilization of the 3+ oxidation state of the metal for $[Fe(bbpen\text{-}Me)]^{3+}$. The opposite situation takes place for $[Fe(bbpen\text{-}NO_2)]^+$, where the 2+ oxidation state of the iron ion is more stabilized by the electron-withdrawing effect of the nitro groups.

Controlled potential coulometry measurements on the $[Fe(bbpen)]^+$ complex in acetonitrile at −1.02 V vs Fc^+/Fc revealed a one-electron reduction process (Fe^{III}/Fe^{II}). The solution changes from deep blue to red, and the cyclic voltammograms of the reduced solution and $[Fe(bbpen)]^+$ are identical under the same experimental conditions. A one-electron reduction for the Fe^{III}/Fe^{II} couple was also observed by Orvig and co-workers for $[Fe(bbpen)]^+$.[15] However, the redox potential they reported is $E_{1/2} = -0.47$ V vs SCE, or −0.63 V vs Fc^+/Fc, which differs by 0.21 V from the value of $E_{1/2} = -0.84$ V vs Fc^+/Fc that we found. The conversion between the standard electrode SCE and the internal standard ferrocene was performed by taking into account the values of $Fc^+/Fc = 0.40$ V vs NHE and SCE = 0.24 V vs NHE.[12,20]

A spectroelectrochemical study, under the same experimental conditions employed in the CV and coulometric experiments, was carried out to examine the electronic spectra of $[Fe^{II}(bbpen)]$. During the reduction of $[Fe(bbpen)]^+$, the band at 574 nm disappeared, giving way to a new band at 434 nm ($\epsilon = 3700$ mol^{-1} L cm^{-1}). This new band is assigned to an iron(II)-to-pyridine MLCT transition. The maintenance of isosbestic points in successive spectra strongly suggests the presence of a single product throughout the course of the electrolysis. The observation of a band in the region of 434 nm for an iron(II) compound coordinated to pyridine and phenolate groups is consistent with the assignment of a superposition of phenolate-to-iron(III) and iron(II)-to-pyridine bands in the mixed-valence compounds $[Fe^{III}Fe^{II}(BBPPNOL)(\mu\text{-}OAc)_2]$,[21] $[Fe^{III}Fe^{II}(BBPMP)(\mu\text{-}OAc)_2]\cdot H_2O$,[22] and $[Fe^{III}Fe^{II}(BPMP)(\mu\text{-}OPr)_2]^{2+}$.[23] The application of the Nernst equation to the spectroelectrochemical data provided $E^{0\prime} = -840$ mV vs Fc^+/Fc and $n = 0.8 \pm 0.1$ electrons. These values are in agreement with $E_{1/2} = -842$ mV vs Fc^+/Fc measured by cyclic voltammetry ($E_{1/2}$) and with $n = 1$ electron for the Fe^{III}/Fe^{II} couple established by coulometry.

Theoretical Calculations. The geometry optimization of the four cationic complexes $[Fe(bbpen)]^+$, $[Fe(bbpen\text{-}Me)]^+$, $[Fe(bbpen\text{-}Br)]^+$, and $[Fe(bbpen\text{-}NO_2)]^+$ was performed using Spartan 04 [24] with the B3LYP hybrid density functional theory in combination with the 6-31G(d,p) and LACVP* basis sets. The results for the calculated bond lengths and angles are summarized in Table 1.

A comparison between the experimental and calculated structural data sets (Table 1) shows good agreement. Small differences between the crystal data and theoretical values (less than 0.121 Å for bond lengths and 4.08° for bond angles) are observed, and these can be assigned to the fact that the X-ray structures were measured in a compacted crystalline form whereas the calculations were performed in a vacuum.

A graphical representation of the α-HOMO for each cationic complex is shown in Figure 5. As can be observed, the p orbitals from the phenolate groups and the d orbital from the iron(III) core participate in its formation. On the other hand, only the pyridine rings contribute to the formation of the α-LUMO, depicted in Figure 6.

A linear correlation was obtained (Figure 7) by plotting the calculated energies of the α-HOMO for the complexes and the Hammett parameter (σ_p) for the substituents. It indicates that the observed effects of the substituent groups

(20) Hammerich, O.; Svensmark, B. *Organic Electrochemistry*, 4th ed.; Marcel Dekker: New York, 2001.

(21) Neves, A.; Erthal, S. M. D.; Drago, V.; Griesar, K.; Haase, W. *Inorg. Chim. Acta* **1992**, *197* (2), 121.
(22) Neves, A.; Brito, M. A.; Vencato, I.; Drago, V.; Griesar, K.; Haase, W. *Inorg. Chem.* **1996**, *35* (8), 2360.
(23) Borovik, A. S.; Papaefthymiou, V.; Taylor, L. F.; Anderson, O. P.; Que, L., Jr. *J. Am. Che. Soc.* **1989**, *111* (16), 6183.
(24) *Spartan 04*, Wavefunction Inc.: Irvine, CA, 2004.

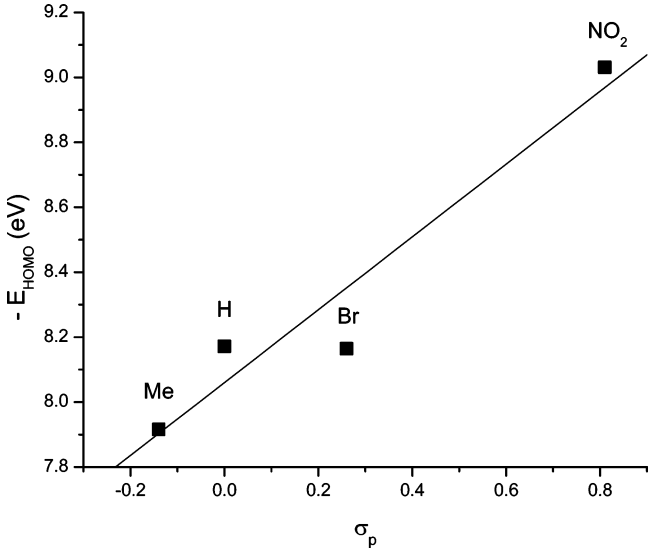

Figure 7. Plot of the calculated energy of α-HOMO (E_{HOMO}) against the Hammett parameter of the substituents (σ_p) for $[Fe(bbpen\text{-}Me)]^+$, $[Fe(bbpen)]^+$, $[Fe(bbpen\text{-}Br)]^+$, and $[Fe(bbpen\text{-}NO_2)]^+$.

on the redox and spectral properties (discussed above) affect the HOMO energies to the same extent. When the energies of the α-HOMO were plotted against the energy of the LMCT process and the redox potential (Figure 8) of the complexes, a trend similar to the experimental correlations shown in Figures 2 and 4 is observed. Thus, this demonstrates that the theoretical calculations describe the electronic behavior of the class of compounds, being in good agreement with the experimental data.

Conclusion

In summary, we have synthesized and studied the structural, spectroscopic, and electrochemical properties of a series of iron(III) complexes with electron-donating and -withdrawing substituents. Linear correlations were obtained when the Fe^{III}/Fe^{II} redox potentials or $O_{phenolate}$-to-iron(III) LMCT processes were plotted against the Hammett parameter for the substituent σ_p values. The redox potential of the $[Fe(bbpen\text{-}NO_2)]^+$ suffered a 411 mV cathodic shift, and its LMCT process was shifted by 58 nm to the blue when compared to the $[Fe(bbpen\text{-}Me)]^+$ complex. These results reveal a significant effect of the substituents on the electronic properties of the complexes, which might be useful in the modulation of properties for enzyme modeling. Theoretical calculations demonstrate that only the pyridine rings contribute to the formation of the LUMO. The HOMO consists of only the phenolate groups, and their interaction with the d orbitals of the metal is observed. Finally, the calculated energies of the α-HOMO also correlate with the Fe^{III}/Fe^{II} redox potentials and $O_{phenolate}$-to-iron(III) LMCT processes, which indicates that the theoretical results agree with the experimental data and are able to describe the electronic properties of the complexes presented.[25]

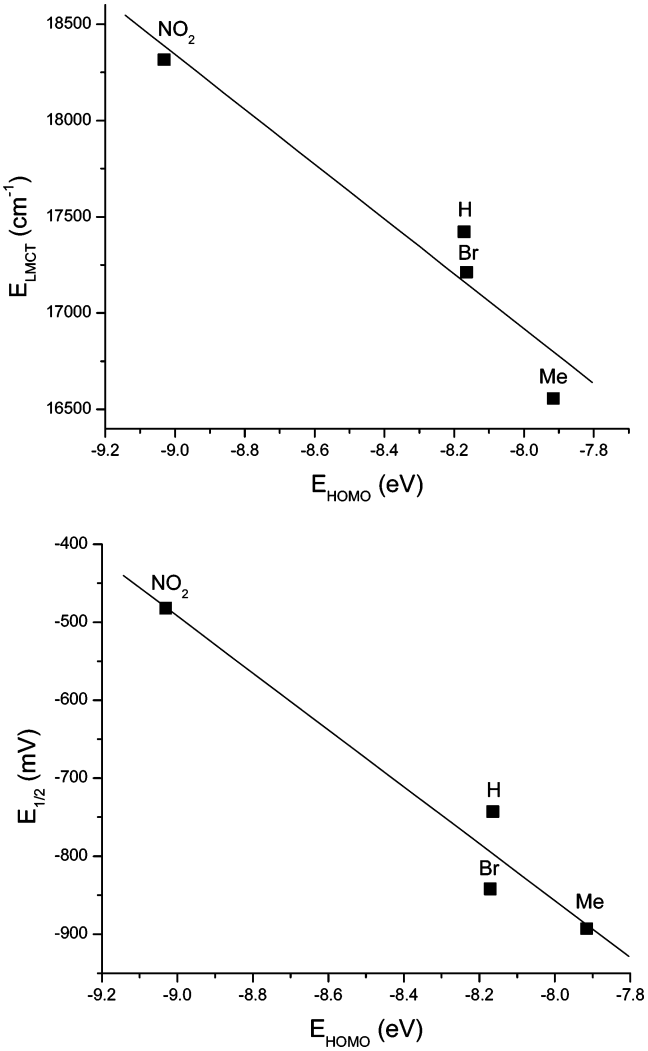

Figure 8. Plots of E_{LMCT} versus E_{HOMO} (left) and $E_{1/2}$ versus E_{HOMO} for $[Fe(bbpen\text{-}Me)]^+$, $[Fe(bbpen)]^+$, $[Fe(bbpen\text{-}Br)]^+$, and $[Fe(bbpen\text{-}NO_2)]^+$. E_{LMCT} refers to the lowest-energy band in the UV−visible spectrum in cm^{-1}; $E_{1/2}$ refers to the redox potential for Fe^{III}/Fe^{II} in mV; E_{HOMO} refers to the calculated energy of the HOMO in eV.

Acknowledgment. Financial support was received from PRONEX, FINEP, and CNPq (Brazil).

Supporting Information Available: Crystallographic data in CIF format. This material is available free of charge via the Internet at http://pubs.acs.org.

IC050869O

(25) Paes, L. W.; Faria, R. B.; Machuca-Herrera, J. O.; Neves, A.; Machado, S. P. *Can. J. Chem.* **2005**, *82*, 1619.